PCCP

ROYAL SOCIETY OF CHEMISTRY

PAPER

View Article Online
View Journal | View Issue

Cite this: *Phys. Chem. Chem. Phys.*, 2020, **22**, 14560

Benchmark *ab initio* characterization of the abstraction and substitution pathways of the OH + CH_4/C_2H_6 reactions

Balázs Gruber and Gábor Czakó *

Received 11th May 2020,
Accepted 22nd June 2020

DOI: 10.1039/d0cp02560g

rsc.li/pccp

We report a comprehensive *ab initio* investigation of the OH + CH_4/C_2H_6 reactions using a high-level composite approach based on CCSD(T)-F12b/aug-cc-pVTZ geometries and CCSD(T)-F12b/aug-cc-pV*n*Z *n* = 5/Q energies augmented with additive corrections of post-CCSD(T) correlation, core correlation, scalar relativity, spin–orbit coupling, and zero-point energy. Besides the hydrogen-abstraction (HA) channel leading to H_2O + CH_3/C_2H_5 (ΔH_0 = −14.37/−18.19 kcal mol^{-1}), we reveal, for the first time, hydrogen-substitution (HS) and methyl-substitution (MS) pathways resulting in H + CH_3OH/C_2H_5OH (ΔH_0 = 13.19/7.12 kcal mol^{-1}) and CH_3 + CH_3OH (ΔH_0 = −2.20 kcal mol^{-1}) products, respectively. The adiabatic barrier heights for HA, MS, and HS in OH + CH_4/C_2H_6 are 4.78/2.18, 39.60, 43.53/41.73(52.48) kcal mol^{-1}, respectively, where substitution proceeds with Walden-inversion or (front-side-attack retention). In the entrance channels van der Waals wells with depths of 0.5–0.8 kcal mol^{-1} are found and in the exit channels the HOH···C_2H_5, HOH···CH_3, H_3C···CH_3OH, and H···C_2H_5OH complexes are characterized with D_e values of 2.4, 1.7, 0.7, and 0.3 kcal mol^{-1}, respectively.

I. Introduction

Moving beyond the reactions of atoms with alkanes,[1–16] the reactions of the OH radical with methane (CH_4) and ethane (C_2H_6) have been thoroughly investigated by theory and experiment to uncover the fundamental rules of polyatomic chemical reactivity.[16–39] The main product channel of the OH + CH_4/C_2H_6 reactions results in H_2O + CH_3/C_2H_5 *via* hydrogen-abstraction (HA). In the early years the kinetics of the OH + CH_4/C_2H_6 reactions were investigated using experimental techniques as well as transition-state theory.[17,18,28,30,31] The stationary points along the HA pathway were characterized by various *ab initio* and density functional methods reporting pre- and post-reaction complexes separated by a transition state for each reaction.[19,22,23,27,28,33,35,38] In the case of the OH + CH_4 system, the CH_4···OH and H_2O···CH_3 complexes were also studied by different experimental techniques using stimulated Raman, infrared and electronic excitation,[24,36,37] photoelectron–photofragment coincidence,[34] and infrared spectroscopy in helium nanodroplets.[26,32] Furthermore, detailed reactive scattering experiments were performed for the different isotope-variants of the OH + CH_4 → H_2O + CH_3 reaction by Liu and co-workers.[29] For the OH + C_2H_6 system, the nascent H_2O vibrational distributions were measured by infrared chemiluminescence.[21] In order to simulate some of the above-mentioned experiments the development of a full-dimensional potential energy surface (PES) was necessary. Following the early work of Espinosa-García and co-workers,[22] Li and Guo[38] developed such a PES for the OH + CH_4 reaction and investigated its dynamics using quasi-classical trajectory and reduced-dimensional quantum methods.[39]

In this study we focus on the high-level *ab initio* characterization of the PES of the OH + CH_4/C_2H_6 reactions providing benchmark structures and energies for the stationary points, thereby complementing our recent work on atom (F, Cl, Br, I) + CH_4/C_2H_6 systems.[13–15] Several aspects of the present study move beyond the previous work: (1) unlike most of the early work except ref. 38, we use the explicitly correlated CCSD(T)-F12 method[40] to obtain structures, frequencies, and energies; (2) basis sets as large as aug-cc-pV5Z (OH + CH_4) and aug-cc-pVQZ (OH + C_2H_6) are employed; (3) post-CCSD(T) correlation effects are considered up to the CCSDT(Q) level of theory; (4) the correlation energy contribution of the core electrons is taken into account; (5) scalar relativistic corrections are determined; and (6) spin–orbit effects are computed. Furthermore, besides the above-mentioned quantitative advances, we investigate several new alternative reaction pathways for the OH + CH_4/C_2H_6 systems, namely hydrogen-substitution and methyl-substitution forming H + CH_3OH/C_2H_5OH and CH_3 + CH_3OH products, respectively. Knowing the energetics of the above

MTA-SZTE Lendület Computational Reaction Dynamics Research Group, Interdisciplinary Excellence Centre and Department of Physical Chemistry and Materials Science, Institute of Chemistry, University of Szeged, Rerrich Béla tér 1, Szeged H-6720, Hungary. E-mail: gczako@chem.u-szeged.hu

channels is essential to develop global PESs for the title reactions and to advance our knowledge on complex reaction mechanisms of multi-channel reactions.

In Section II we describe the computational details of the composite approach used to determine the best technically feasible stationary-point properties. The results are presented and discussed in Section III. The paper ends with summary and conclusions in Section IV.

II. Computational details

Stationary-point search is performed on the basis of previous studies[14,38] and chemical intuition using the second-order Møller–Plesset perturbation theory[41] (MP2) with the aug-cc-pVDZ basis set.[42] The obtained minima and saddle points are further optimized with the explicitly-correlated coupled-cluster singles, doubles, and perturbative triples (CCSD(T)-F12b) method[40] using the aug-cc-pVDZ and aug-cc-pVTZ basis sets.[42] Harmonic vibrational frequencies are computed for each stationary point using the MP2/aug-cc-pVDZ, CCSD(T)-F12b/aug-cc-pVDZ, and CCSD(T)-F12b/aug-cc-pVTZ (except for some of the OH + C_2H_6 stationary points) levels of theory.

In order to achieve sub-chemical accuracy we perform the following singe-point energy computations at the best geometries obtained at the CCSD(T)-F12b/aug-cc-pVTZ level:

(1) CCSD(T)-F12b computations are carried out using the aug-cc-pVQZ and, in the case of the OH + CH_4 system, the aug-cc-pV5Z basis sets.

(2) CCSD(T),[43] CCSDT,[44] and CCSDT(Q)[45] methods are used with the cc-pVDZ and, in the case of the OH + CH_4 system, the aug-cc-pVDZ basis sets.

(3) All-electron (AE) and frozen-core (FC) computations are performed at the CCSD(T)-F12b/cc-pCVTZ-F12 level of theory.[40,46] In the usual FC treatment only the valence electrons are correlated, whereas the AE computations correlate the $1s^2$ electrons of the C and O atoms as well.

(4) Second-order Douglas–Kroll[47] (DK) relativistic energies are computed at the AE-CCSD(T)-F12b/cc-pCVTZ-F12 level of theory.

(5) Spin–orbit (SO) corrections are determined using the Breit–Pauli Hamiltonian in the interacting-states approach[48] using the Davidson-corrected[49] multi-reference configuration interaction[50] (MRCI+Q) method with the aug-cc-pVDZ and aug-cc-pVTZ basis sets. The MRCI computations utilize an active space of 15/21 electrons in 8/11 spatial orbitals keeping all the 4/6 core electrons frozen for OH + CH_4/C_2H_6. Two doubly-degenerate electronic states are determined, non-SO_1 and non-SO_2, resulting in a 4 × 4 SO matrix, whose eigenvalues correspond to the two-fold ground (SO_1) and excited (SO_2) spin–orbit states.

The benchmark classical relative energies are calculated by the following composite energy expression:

$$\text{CCSD(T)-F12b/aug-cc-pV}n\text{Z} + \delta[\text{CCSDT}] + \delta[\text{CCSDT(Q)}] + \Delta_{\text{core}} + \Delta_{\text{rel}} + \Delta_{\text{SO}}, \quad (1)$$

where n = 5 and 4(Q) for the OH + CH_4 and OH + C_2H_6 systems, respectively, and

$$\delta[\text{CCSDT}] = \text{CCSDT/(aug-)cc-pVDZ} - \text{CCSD(T)/(aug-)cc-pVDZ}, \quad (2)$$

$$\delta[\text{CCSDT(Q)}] = \text{CCSDT(Q)/(aug-)cc-pVDZ} - \text{CCSDT/(aug-)cc-pVDZ}, \quad (3)$$

$$\Delta_{\text{core}} = \text{AE-CCSD(T)-F12b/cc-pCVTZ-F12} - \text{FC-CCSD(T)-F12b/cc-pCVTZ-F12}, \quad (4)$$

$$\Delta_{\text{rel}} = \text{DK-AE-CCSD(T)-F12b/cc-pCVTZ-F12} - \text{AE-CCSD(T)-F12b/cc-pCVTZ-F12} \quad (5)$$

$$\Delta_{\text{SO}} = \text{SO}_1\text{(MRCI+Q/aug-cc-pVTZ)} - \text{non-SO}_1\text{(MRCI+Q/aug-cc-pVTZ)}. \quad (6)$$

The benchmark adiabatic relative energies are obtained as

$$\text{CCSD(T)-F12b/aug-cc-pV}n\text{Z} + \delta[\text{CCSDT}] + \delta[\text{CCSDT(Q)}] + \Delta_{\text{core}} + \Delta_{\text{rel}} + \Delta_{\text{SO}} + \Delta_{\text{ZPE}} \quad (7)$$

including the terms defined in eqn (1)–(6) and the zero-point energy correction (Δ_{ZPE}) determined at the CCSD(T)-F12b/aug-cc-pVTZ level, except for some of the OH + C_2H_6 stationary points, where the frequency computations are performed without symmetry at the CCSD(T)-F12b/aug-cc-pVDZ level.

For open-shell systems the MP2 method is used in a restricted formalism (RMP2),[51] unless otherwise noted, whereas all the CCSD(T)-F12b computations utilize the unrestricted UCCSD(T)-F12b[52] method based on restricted open-shell Hartree–Fock (ROHF) orbitals. For the determination of the post-CCSD(T) correlation effects we use unrestricted Hartree–Fock (UHF) reference and the unrestricted UCCSD(T), UCCSDT, and UCCSDT(Q) methods. Note that, for the sake of simplicity, we usually omit the reference function as well as the R (restricted) and U (unrestricted) abbreviations in the notations.

All the MP2, CCSD(T)-F12b, MRCI, and SO computations are carried out with the Molpro program package,[53] whereas the CCSD(T), CCSDT, and CCSDT(Q) energies are obtained with Mrcc[54] interfaced to Molpro.

III. Results and discussion

The topology of the PESs with the benchmark classical and adiabatic energies of the OH + CH_4 and OH + C_2H_6 reactions are shown in Fig. 1 and 2, respectively, and the corresponding stationary-point geometries showing the most important structural parameters at different levels of theory are given in Fig. 3 and 4. The HA pathways are exothermic with benchmark classical(adiabatic) $\Delta E(\Delta H_0)$ values of −13.07(−14.37)/−16.70(−18.19) kcal mol^{-1} for the OH($^2\Pi_{3/2}$) + CH_4/C_2H_6 → H_2O + CH_3/C_2H_5 reactions. The HA barrier is significantly higher for OH + CH_4, *i.e.*, 6.30(4.78) kcal mol^{-1} than in the case of OH + C_2H_6, 3.69(2.18) kcal mol^{-1}. The structures of the hydrogen-abstraction transition-states (HA TSs) are reactant like in both cases as the reactive C–H bonds are only stretched by 0.118/0.087 Å relative to the corresponding bond lengths in

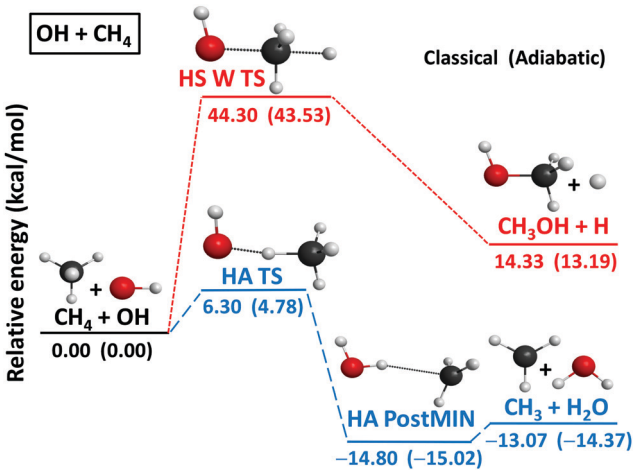

Fig. 1 Schematic potential energy surface of the OH($^2\Pi_{3/2}$) + CH_4 reaction showing the benchmark classical (adiabatic) relative energies of the stationary points along the different reaction pathways.

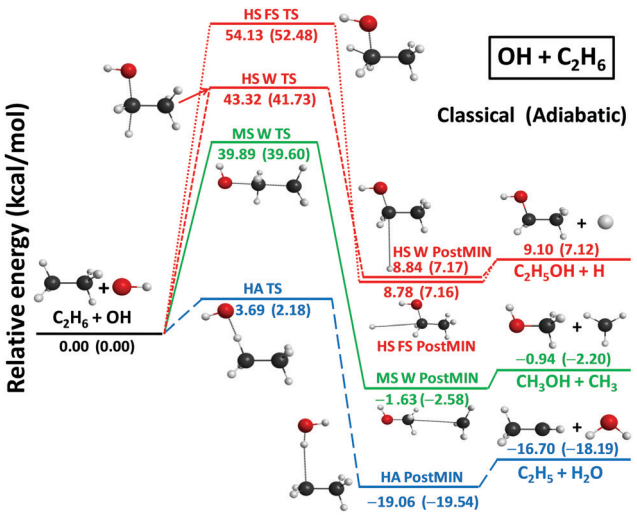

Fig. 2 Schematic potential energy surface of the OH($^2\Pi_{3/2}$) + C_2H_6 reaction showing the benchmark classical (adiabatic) relative energies of the stationary points along the different reaction pathways.

CH_4/C_2H_6, whereas the forming O–H bonds are stretched by 0.363/0.428 Å relative to the H_2O product as shown in Fig. 3 and 4. Thus, the exothermic HA processes feature early barriers in accord with the Hammond postulate[55] and the more exothermic OH + C_2H_6 reaction has lower and more reactant-like barrier as the above-discussed data show. In the product wells of both systems there are post-reaction minima (HA PostMINs), where H_2O binds to the CH_3/C_2H_5 units with a single hydrogen-bond. The $D_e(D_0)$ values of the HA PostMIN complexes are 1.73(0.65)/2.36(1.35) kcal mol^{-1}, in accord with the ratio of the intermolecular C···H distances of 2.383/2.312 Å. The greater stability of the latter can be explained by the fact that the C_2H_5 unit has larger dipole moment than the CH_3 fragment.

For the OH + CH_4 reaction we have found an endothermic, $\Delta E(\Delta H_0)$ = 14.33(13.19) kcal mol^{-1}, hydrogen-substitution (HS) pathway resulting in H + CH_3OH products *via* a Walden-inversion TS (HS W TS) with a classical(adiabatic) barrier height of 44.30(43.53) kcal mol^{-1} as shown in Fig. 1. The HS W TS has C_s symmetry with nearly collinear O–C–H arrangement, where the O–C and C–H distances are 1.717 and 1.415 Å, respectively, stretched by 0.297 and 0.327 Å relative the corresponding bonds in CH_3OH and CH_4 (Fig. 3); thus, HS has a central or slightly-late barrier. The HS pathway of the OH + CH_4 reaction is revealed for the first time in the present study, but for atom + methane reactions HS is not unprecedented.[4,56–60] For the H and O(^{3}P) + CH_4 reactions HS was investigated both experimentally[4,56] and theoretically.[4,57] For Cl + CH_4 we found a Walden-inversion barrier height of 42.08(38.84) kcal mol^{-1},[58] which is similar to that of OH + CH_4. Besides Walden inversion, for the O(^{3}P) and Cl + CH_4 reactions front-side attack TSs with C_{2v} and C_{4v} symmetry, respectively, were reported.[4,60] In the case of OH + CH_4 we do not find front-side attack TS; however, reaction dynamics simulations may reveal retention trajectories as we found that the retention pathways of the Cl + CH_4 → H + CH_3Cl reaction avoid the high-energy C_{4v} TS.[60]

In the case of the OH + C_2H_6 reaction HS pathways leading to H + C_2H_5OH also exist as shown in Fig. 2. The endothermicity of the HS channel, $\Delta E(\Delta H_0)$ = 9.10(7.12) kcal mol^{-1}, is less than that of the OH + CH_4 reaction, $\Delta E(\Delta H_0)$ = 14.33(13.19) kcal mol^{-1}, whereas the Walden-inversion classical(adiabatic) barrier heights of the two systems are similar, *i.e.*, 43.32(41.73) kcal mol^{-1} for OH + C_2H_6 and 44.30(43.53) kcal mol^{-1} for OH + CH_4. Furthermore, these HS barrier heights are also very similar to that of the Cl + C_2H_6 system, 41.60(37.66) kcal mol^{-1}.[14] For the OH + C_2H_6 reaction we have found a front-side (FS) attack retention pathway *via* a higher barrier with classical(adiabatic) height of 54.13(52.48) kcal mol^{-1}.[14] At the HS W TS the forming O–C and breaking C–H bonds are nearly collinear (168.3°) and the H_2C–C unit is almost planar, whereas at the HS FS TS the O–C–H angle is 58.2° along the reaction coordinate and the H_2C–CH_3 unit is ethane-like retaining its reactant configuration. Similar HS FS TS was found for the X + C_2H_6 [X = F, Cl, Br, I] reactions, comparing the barrier heights again the X = Cl case has similar, though slightly larger, value of 59.14(54.97) kcal mol^{-1}. For the OH + C_2H_6 reaction we have found weakly-bound H···C_2H_5OH complexes in the exit channels of the HS inversion and retention pathways with small D_e values of 0.26 and 0.32 kcal mol^{-1}, respectively. However, these shallow HS product-channel wells may not support a bound vibrational state, because the ZPE-corrected energies of the HS W PostMIN and HS FS PostMIN complexes are slightly above the vibrationally ground-state product asymptote by 0.05 and 0.04 kcal mol^{-1} (Fig. 2).

Unlike for OH + CH_4, for the OH + C_2H_6 reaction a third product channel is possible resulting in CH_3OH + CH_3 *via* methyl substitution (MS). As Fig. 2 shows, MS is slightly exothermic $\Delta E(\Delta H_0)$ = −0.94(−2.20) kcal mol^{-1} and goes over a classical (adiabatic) Walden-inversion barrier of 39.89(39.60) kcal mol^{-1} height. Thus, similarly to the halogen + C_2H_6 reactions,[14] MS is both thermodynamically and kinetically favored over HS. At the central MS W TS the O–C–C atoms are nearly collinear and the forming O–C and breaking C–C bonds are stretched by 0.407 and 0.413 Å, respectively, relative to their corresponding equilibrium

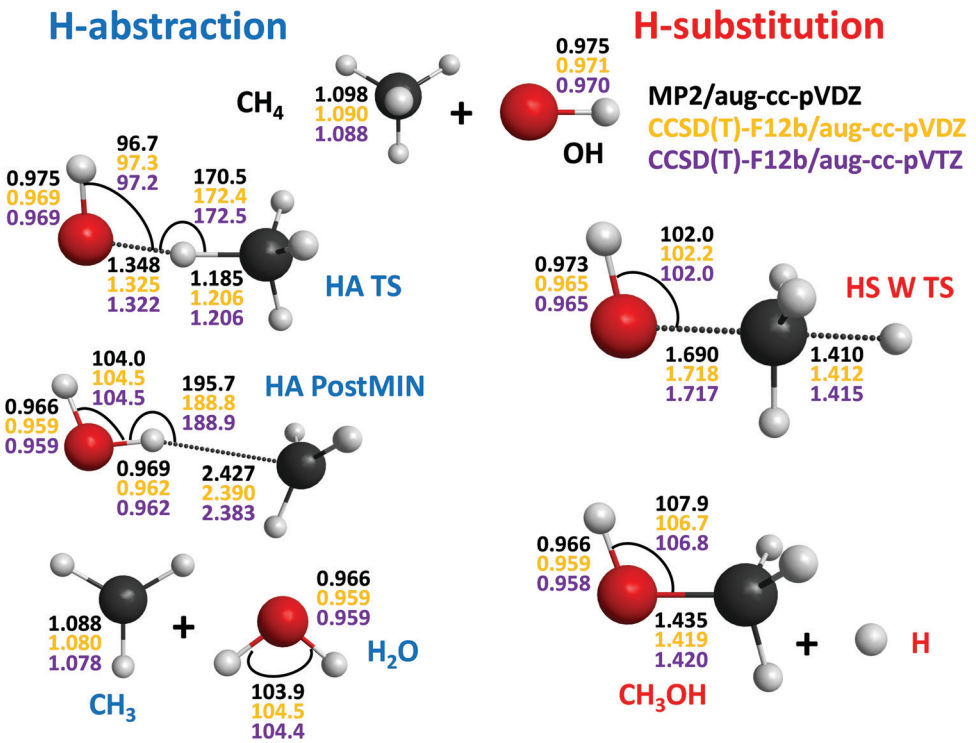

Fig. 3 Stationary-point structures of the OH + CH_4 system showing the most important distances (Å) and angles (degree) obtained at the MP2/aug-cc-pVDZ, CCSD(T)-F12b/aug-cc-pVDZ, and CCSD(T)-F12b/aug-cc-pVTZ levels of theory.

values in the product and reactant (Fig. 4). For the halogen + C_2H_6 systems we reported a higher-energy front-side attack MS pathway as well,[14] however, for OH + C_2H_6 MS FS TS is not found, though its existence cannot be ruled out. Nevertheless, we have found a $H_3C\cdots CH_3OH$ complex in the product channel of MS with $D_e(D_0)$ values of 0.69(0.38) kcal mol^{-1}. The stability trend, D_e = {2.4, 0.7, 0.3} kcal mol^{-1}, of the {HA, MS, HS} PostMIN complexes, {$HOH\cdots C_2H_5$, $H_3C\cdots CH_3OH$, $H\cdots C_2H_5OH$}, reflects the facts that HA PostMIN is stabilized by dipole–dipole interaction and CH_3 is more polarizable than the H atom.

The above-discussed stationary-point properties correspond to our new benchmark values obtained by the composite *ab initio* approach described in Section II. Now let us discuss the accuracy of the computed results. The most important structural parameters of the stationary points obtained by the MP2/aug-cc-pVDZ, CCSD(T)-F12b/aug-cc-pVDZ, and CCSD(T)-F12b/aug-cc-pVTZ levels of theory are shown in Fig. 3 and 4. As seen, the MP2 and CCSD(T)-F12b results may differ by about 0.01 Å, whereas the CCSD(T)-F12b distances with the aug-cc-pVDZ and aug-cc-pVTZ basis sets usually agree within 0.001 Å, except for large intermolecular distances where an order of magnitude larger uncertainties are found due to the flatness of the potential along the dissociation coordinate.

The convergence of the relative energies are shown in Tables 1 and 2 for the OH + CH_4 and OH + C_2H_6 systems, respectively, and the corresponding auxiliary corrections are detailed in Tables 3 and 4. The MP2 and CCSD(T)-F12b relative energies differ by 1–6 kcal mol^{-1}, for example, MP2 overestimates the HA barrier heights by 2.4–2.8 kcal mol^{-1} and underestimates the endoergicity of the HS channels by 5.8–6.0 kcal mol^{-1} as seen in Tables 1 and 2. Thus, it is clear that the use of the CCSD(T)-F12b method is needed to achieve chemical accuracy (uncertainty less than 1 kcal mol^{-1}). For the OH + CH_4 system we have CCSD(T)-F12b energies up to the large aug-cc-pV5Z basis and on the basis of Table 1 we find that the average absolute deviations of the aug-cc-pVDZ, aug-cc-pVTZ, and aug-cc-pVQZ relative energies from the aug-cc-pV5Z data decrease as 0.25, 0.06, 0.04 kcal mol^{-1}, respectively, showing the excellent basis convergence of the explicitly-correlated CCSD(T)-F12b method. Thus, we expect that even the CCSD(T)-F12b/aug-cc-pVQZ result is basis converged within 0.1 kcal mol^{-1}. This finding for OH + CH_4 is useful for the larger OH + C_2H_6 system, where we do not perform the CCSD(T)-F12b/aug-cc-pV5Z computations. For OH + C_2H_6, the aug-cc-pVDZ and aug-cc-pVTZ CCSD(T)-F12b relative energies are converged with average absolute deviations of 0.27 and 0.04 kcal mol^{-1}, respectively, with respect to the CCSD(T)-F12b/aug-cc-pVQZ results.

The large-basis CCSD(T)-F12b computations provide a very good estimate of the complete-basis-set limit of the CCSD(T) relative energies. If one aims to approach the "exact" energies additional small corrections, such as post-CCSD(T) and core electron correlation as well as scalar and SO relativistic effects should be considered. Furthermore, to get experimentally observable quantities the ZPE corrections have to be taken into account. These so-called auxiliary corrections are given in Tables 3 and 4 for the OH + CH_4 and OH + C_2H_6 systems, respectively. For OH + CH_4 we have determined the δ[CCSDT]

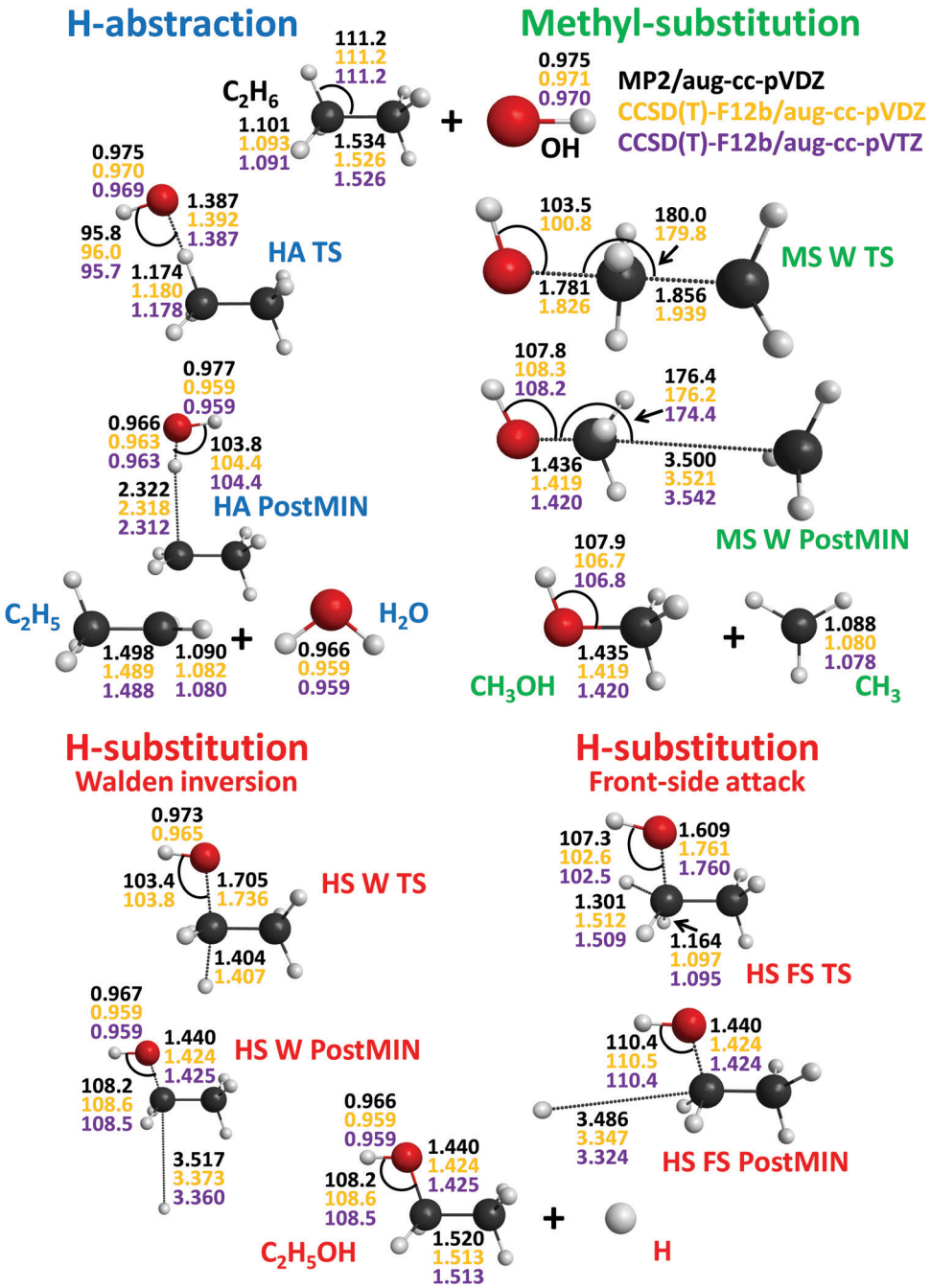

Fig. 4 Stationary-point structures of the OH + C_2H_6 system showing the most important distances (Å) and angles (degree) obtained at the MP2/aug-cc-pVDZ (see footnote *k* of Table 2), CCSD(T)-F12b/aug-cc-pVDZ, and CCSD(T)-F12b/aug-cc-pVTZ levels of theory.

and δ[CCSDT(Q)] corrections with the cc-pVDZ and aug-cc-pVDZ basis sets. As Table 3 shows even the small cc-pVDZ basis provides good estimates for these post-CCSD(T) correlation effects suggesting that it is sufficient to perform only the CCSDT(Q)/cc-pVDZ computations for the larger OH + C_2H_6 system. In the case of the products and HA PostMIN of the OH + CH_4 reaction the δ[CCSDT] and δ[CCSDT(Q)] absolute corrections are between 0–0.2 kcal mol^{-1} and partially cancel each other. However, for the HA TS and HS W TS the aug-cc-pVDZ(cc-pVDZ) corrections add up to −0.35(−0.26) and −0.61(−0.61) kcal mol^{-1}, respectively, showing the good performance of the smaller basis set. For the OH + C_2H_6 system most of the post-CCSD(T) corrections have the same negative sign, except the HS products and PostMINs (Table 4). The largest cumulative post-CCSD(T) corrections are found for the TSs, namely −0.25, −0.67, −0.88, and −0.91 kcal mol^{-1}, for HA TS, HS W TS, HS FS TS, and MS W TS, respectively, which are clearly not negligible if sub-chemical accuracy is desired.

For both reactions the core correlation corrections are in the range from −0.11 to +0.39 kcal mol^{-1}, whereas the scalar

Table 1 Energies (kcal mol^{-1}) of the stationary points and product channels of the OH + CH_4 reaction relative to the reactants at different levels of theory

	MP2	CCSD(T)-F12b							
Stationary points	aVDZ[a]	aVDZ[b]	aVTZ[c]	aVQZ[d]	aV5Z[e]	$\sum\Delta$[f]	Classical[g]	Δ_{ZPE}[h]	Adiabatic[i]
HA TS	8.50	6.08	6.27	6.30	6.38	−0.08	6.30	−1.52	4.78
HA PostMIN	−18.22	−15.15	−14.99	−15.00	−14.96	+0.16	−14.80	−0.22	−15.02
HS W TS	41.07	44.52	44.40	44.38	44.42	−0.12	44.30	−0.77	43.53
CH_3OH + H	7.62	13.39	14.00	13.95	13.98	+0.35	14.33	−1.14	13.19
CH_3 + H_2O	−16.28	−13.19	−13.15	−13.25	−13.25	+0.18	−13.07	−1.30	−14.37

[a] MP2/aug-cc-pVDZ relative energies obtained at MP2/aug-cc-pVDZ geometries. [b] CCSD(T)-F12b/aug-cc-pVDZ relative energies obtained at CCSD(T)-F12b/aug-cc-pVDZ geometries. [c] CCSD(T)-F12b/aug-cc-pVTZ relative energies obtained at CCSD(T)-F12b/aug-cc-pVTZ geometries. [d] CCSD(T)-F12b/aug-cc-pVQZ relative energies obtained at CCSD(T)-F12b/aug-cc-pVTZ geometries. [e] CCSD(T)-F12b/aug-cc-pV5Z relative energies obtained at CCSD(T)-F12b/aug-cc-pVTZ geometries. [f] $\sum\Delta = \delta$[CCSDT/aVDZ] + δ[CCSDT(Q)/aVDZ] + Δ_{core} + Δ_{rel} + Δ_{SO}(aVTZ). [g] Benchmark classical relative energy obtained as CCSD(T)-F12b/aV5Z + $\sum\Delta$. [h] ZPE correction obtained at CCSD(T)-F12b/aug-cc-pVTZ. [i] Benchmark adiabatic relative energy obtained as classical + Δ_{ZPE}.

Table 2 Energies (kcal mol^{-1}) of the stationary points and product channels of the OH + C_2H_6 reaction relative to the reactants at different levels of theory

	MP2	CCSD(T)-F12b						
Stationary points	aVDZ[a]	aVDZ[b]	aVTZ[c]	aVQZ[d]	$\sum\Delta$[e]	Classical[f]	Δ_{ZPE}[g]	Adiabatic[h]
HA TS	6.21	3.45	3.65	3.70	−0.01	3.69	−1.51	2.18
HA PostMIN	−21.78	−19.28	−19.07	−19.09	+0.03	−19.06	−0.48	−19.54
HS W TS	39.89	43.57	43.49[i]	43.51[i]	−0.19	43.32	−1.59[j]	41.73
HS W PostMIN	2.11	7.96	8.62	8.63	+0.21	8.84	−1.67	7.17
HS FS TS	55.68[k]	54.33	54.47	54.53	−0.40	54.13	−1.65[j]	52.48
HS FS PostMIN	2.00[k]	7.90	8.56	8.57	+0.21	8.78	−1.62[j]	7.16
MS W TS	44.80[k]	40.29	40.21[i]	40.21[i]	−0.32	39.89	−0.29[j]	39.60
MS W PostMIN	−3.14[k]	−2.02	−1.85	−1.89	+0.26	−1.63	−0.95[j]	−2.58
C_2H_5OH + H	2.29	8.29	8.91	8.89	+0.21	9.10	−1.98	7.12
CH_3OH + CH_3	−2.24	−1.16	−1.13	−1.21	+0.27	−0.94	−1.26	−2.20
C_2H_5 + H_2O	−18.96	−16.64	−16.61	−16.75	+0.05	−16.70	−1.49	−18.19

[a] MP2/aug-cc-pVDZ relative energies obtained at MP2/aug-cc-pVDZ geometries. [b] CCSD(T)-F12b/aug-cc-pVDZ relative energies obtained at CCSD(T)-F12b/aug-cc-pVDZ geometries. [c] CCSD(T)-F12b/aug-cc-pVTZ relative energies obtained at CCSD(T)-F12b/aug-cc-pVTZ geometries. [d] CCSD(T)-F12b/aug-cc-pVQZ relative energies obtained at CCSD(T)-F12b/aug-cc-pVTZ geometries. [e] $\sum\Delta = \delta$[CCSDT] + δ[CCSDT(Q)] + Δ_{core} + Δ_{rel} + Δ_{SO}(aVTZ). [f] Benchmark classical relative energy obtained as CCSD(T)-F12b/aVQZ + $\sum\Delta$. [g] ZPE correction obtained at CCSD(T)-F12b/aug-cc-pVTZ (for exemptions see *j*). [h] Benchmark adiabatic relative energy obtained as classical + Δ_{ZPE}. [i] Obtained at CCSD(T)-F12b/aug-cc-pVDZ geometries. [j] ZPE correction obtained at CCSD(T)-F12b/aug-cc-pVDZ. [k] Obtained with UMP2.

Table 3 Auxiliary corrections (kcal mol^{-1}) for the relative energies of the stationary points and product channels of the OH + CH_4 reaction

	δ[CCSDT][a]		δ[CCSDT(Q)][b]				Δ_{SO}[e]		Δ_{ZPE}[f]		
Stationary points	VDZ	aVDZ	VDZ	aVDZ	Δ_{core}[c]	Δ_{rel}[d]	aVDZ	aVTZ	MP2/DZ	CC/DZ	CC/TZ
HA TS	−0.11	−0.12	−0.15	−0.23	0.06	0.02	0.18	0.19	−1.05	−1.67	−1.52
HA PostMIN	0.00	0.04	−0.13	−0.15	−0.04	0.12	0.18	0.19	−0.06	−0.01	−0.22
HS W TS	−0.26	−0.18	−0.35	−0.43	0.25	0.05	0.17	0.19	−0.75	−0.84	−0.77
CH_3OH + H	0.09	0.18	−0.20	−0.19	0.02	0.15	0.18	0.19	−1.24	−1.12	−1.14
CH_3 + H_2O	0.01	0.05	−0.13	−0.14	−0.04	0.12	0.18	0.19	−1.26	−1.26	−1.30

[a] CCSDT – CCSD(T) obtained with the cc-pVDZ (VDZ) and aug-cc-pVDZ (aVDZ) basis sets at CCSD(T)-F12b/aug-cc-pVTZ geometries. [b] CCSDT(Q) – CCSDT obtained with the cc-pVDZ (VDZ) and aug-cc-pVDZ (aVDZ) basis sets at CCSD(T)-F12b/aug-cc-pVTZ geometries. [c] Core-correlation correction obtained as the difference between all-electron and frozen-core CCSD(T)-F12b/cc-pCVTZ-F12 relative energies at CCSD(T)-F12b/aug-cc-pVTZ geometries. [d] Scalar relativistic effect obtained as the difference between Douglas–Kroll and non-relativistic all-electron CCSD(T)-F12b/cc-pCVTZ-F12 relative energies at CCSD(T)-F12b/aug-cc-pVTZ geometries. [e] Spin–orbit (SO) corrections obtained as the difference between the SO and non-SO ground-state MRCI+Q/aug-cc-pVDZ (aVDZ) or MRCI+Q/aug-cc-pVTZ (aVTZ) relative energies at CCSD(T)-F12b/aug-cc-pVTZ geometries. [f] ZPE corrections obtained at MP2/aug-cc-pVDZ (MP2/DZ), CCSD(T)-F12b/aug-cc-pVDZ (CC/DZ), and CCSD(T)-F12b/aug-cc-pVTZ (CC/TZ).

relativistic effects on the relative energies are always small positive values between 0.01 and 0.15 kcal mol^{-1}. The largest core corrections are obtained for the HS TSs (0.24–0.26 kcal mol^{-1}) and for the MS W TS (0.39 kcal mol^{-1}) as seen in Tables 3 and 4.

SO interaction almost fully quenches at all the stationary points, while lowers the reactant asymptote, thereby increasing all the relative energies by 0.19 kcal mol^{-1}. As seen in Tables 3 and 4 we have performed SO computations with the aug-cc-

Table 4 Auxiliary corrections (kcal mol^{-1}) for the relative energies of the stationary points and product channels of the OH + C_2H_6 reaction

					Δ_{SO}[e]		Δ_{ZPE}[f]		
Stationary points	δ[CCSDT][a]	δ[CCSDT(Q)][b]	Δ_{core}[c]	Δ_{rel}[d]	aVDZ	aVTZ	MP2/DZ	CC/DZ	CC/TZ
HA TS	−0.11	−0.14	0.03	0.02	0.18	0.19	−2.08	−1.74	−1.51
HA PostMIN	−0.04	−0.13	−0.11	0.12	0.18	0.19	−0.08	−0.31	−0.48
HS W TS	−0.27[g]	−0.40[g]	0.24[g]	0.05[g]	0.18[g]	0.19[g]	−1.55	−1.59	
HS W PostMIN	0.10	−0.20	−0.02	0.14	0.18	0.19	−1.82	−1.69	−1.67
HS FS TS	−0.38	−0.50	0.26	0.03	0.18	0.19	−1.88[h]	−1.65	
HS FS PostMIN	0.10	−0.20	−0.02	0.14	0.18	0.19	−1.80[h]	−1.62	
MS W TS	−0.48[g]	−0.43[g]	0.39[g]	0.01[g]	0.18[g]	0.19[g]	1.19[h]	−0.29	
MS W PostMIN	−0.02	−0.12	0.09	0.12	0.18	0.19	−0.84[h]	−0.95	
C_2H_5OH + H	0.10	−0.20	−0.02	0.14	0.18	0.19	−2.08	−1.92	−1.98
CH_3OH + CH_3	−0.02	−0.11	0.09	0.12	0.18	0.19	−1.15	−1.21	−1.26
C_2H_5 + H_2O	−0.03	−0.12	−0.11	0.12	0.18	0.19	−1.51	−1.47	−1.49

[a] CCSDT – CCSD(T) obtained with the cc-pVDZ basis set at CCSD(T)-F12b/aug-cc-pVTZ geometries. [b] CCSDT(Q) – CCSDT obtained with the cc-pVDZ basis set at CCSD(T)-F12b/aug-cc-pVTZ geometries. [c] Core-correlation correction obtained as the difference between all-electron and frozen-core CCSD(T)-F12b/cc-pCVTZ-F12 relative energies at CCSD(T)-F12b/aug-cc-pVTZ geometries. [d] Scalar relativistic effect obtained as the difference between Douglas–Kroll and non-relativistic all-electron CCSD(T)-F12b/cc-pCVTZ-F12 relative energies at CCSD(T)-F12b/aug-cc-pVTZ geometries. [e] Spin–orbit (SO) corrections obtained as the difference between the SO and non-SO ground-state MRCI+Q/aug-cc-pVDZ (aVDZ) or MRCI+Q/aug-cc-pVTZ (aVTZ) relative energies at CCSD(T)-F12b/aug-cc-pVTZ geometries. [f] ZPE corrections obtained at MP2/aug-cc-pVDZ (MP2/DZ), CCSD(T)-F12b/aug-cc-pVDZ (CC/DZ), and CCSD(T)-F12b/aug-cc-pVTZ (CC/TZ). [g] Obtained at CCSD(T)-F12b/aug-cc-pVDZ geometries. [h] Obtained with UMP2.

pVDZ and aug-cc-pVTZ basis sets, which result in almost the same corrections of 0.18 (once 0.17) and 0.19 kcal mol^{-1}, respectively. These values are in good agreement with the experimental data of 0.20 kcal mol^{-1} deduced from the measured SO splitting (ε = 0.40 kcal mol^{-1}) of the OH radical as ε/2. To get deeper insight, we have computed SO and non-SO potential energy curves along the intermolecular coordinates of the $CH_4\cdots$OH and $C_2H_6\cdots$OH systems while the OH approaches the CH_4 and C_2H_6 molecules from different directions as shown in Fig. 5 and 6. The ground electronic state of the OH radical is the 2 × 2-fold degenerate $^2\Pi$, which splits to a 2-fold SO ground ($^2\Pi_{3/2}$) and a 2-fold SO excited state ($^2\Pi_{1/2}$). As OH approaches CH_4 the two doublet non-SO state remains quasi-degenerate and the SO ground and excited states are below and above the non-SO states by ε/2 as shown in Fig. 5. There is a van der Waals well in the entrance channel whose depth is 0.5 and 0.7 kcal mol^{-1} with $HCH_3\cdots$OH and $H_3CH\cdots$OH C_{3v} orientations, respectively. The well depths and positions are not affected by the SO interaction, because the wells are at C$\cdots$O distances of 3–4 Å, whereas the SO correction is almost constant until the C$\cdots$O distance decreases to about 2 Å, where the difference between the SO and non-SO ground state energies rapidly drops to zero (see insets in Fig. 5). This fast quenching of SO interaction occurs at high relative energies above 100 kcal mol^{-1}, where the quasi-degeneracy of the non-SO states starts lifting. Interestingly, in the case of the halogen (X) + CH_4 reactions, the $HCH_3\cdots$X minimum is the deeper with depth of 0.6(0.9) kcal mol^{-1} and the $H_3CH\cdots$X well is the shallower, 0.3(0.3) kcal mol^{-1}, with(without) SO correction.[13,58] In the case of the $H_3CCH_3\cdots$OH (C_{3v}) and $H_3CH_2CH\cdots$OH (C_s) arrangements in the entrance well of OH + C_2H_6 reaction, the conclusions are qualitatively the same as for OH + CH_4, *i.e.*, the former minimum is 0.6 kcal mol^{-1} deep, whereas the latter is deeper, 0.7 kcal mol^{-1}, and these are not affected by the SO interactions. If OH approaches C_2H_6 perpendicularly to the C–C bond, the well is the deepest, 0.8 kcal mol^{-1}, and slightly affected by the SO interaction as the quenching and the departure of the two non-SO states occur in the 2.5–3.5 Å range of the CC$\cdots$O distance as seen in Fig. 6. For the X + C_2H_6 systems, the $H_3CCH_3\cdots$X (C_{3v}) minimum was found to be the deepest, slightly below the perpendicular well, and the $H_3CH_2CH\cdots$X (C_s) arrangement gave the shallowest minimum.[14] These entrance-channel wells may play an important role in the dynamics of the title reactions at low collision energies, especially for OH + C_2H_6, which has a low barrier for HA.

The ZPE effects on the relative energies are always negative and in the most cases the absolute corrections are in the range of 1–2 kcal mol^{-1} as shown in Tables 1 and 2. The mean absolute deviation of the MP2 ZPE corrections from the CCSD(T)-F12b results is about 0.2 kcal mol^{-1}, whereas the CCSD(T)-F12b/aug-cc-pVTZ data are converged within 0.1 kcal mol^{-1} as Tables 3 and 4 show. These ZPE effects are clearly not negligible if we aim to compute chemically accurate, measurable adiabatic relative energies.

For the reaction enthalpies comparison between the present computed adiabatic relative energies and the ''experimental'' data deduced from 0 K enthalpies of formation taken from the Active Thermochemical Tables (ATcT)[61] is possible. Note that ATcT collects the best measured and computed thermochemical data, thereby providing the best available predictions for enthalpies of formation and their uncertainties of several chemical species. We call these ATcT data as ''experimental'' even if they rely on both theory and experiment. As Table 5 shows the agreement between the present *ab initio* 0 K reaction enthalpies and experiment is excellent; the mean absolute deviation between theory and experiment is only 0.07 kcal mol^{-1} and, in most cases, the theoretical predictions are within the error bars of the experiment. This comparison demonstrates that one needs to consider the auxiliary corrections (post-CCSD(T), core, scalar relativistic, SO) to achieve this outstanding accuracy, because the cumulative effect of these corrections averaged for the five reaction channels is 0.21 kcal mol^{-1}, which is

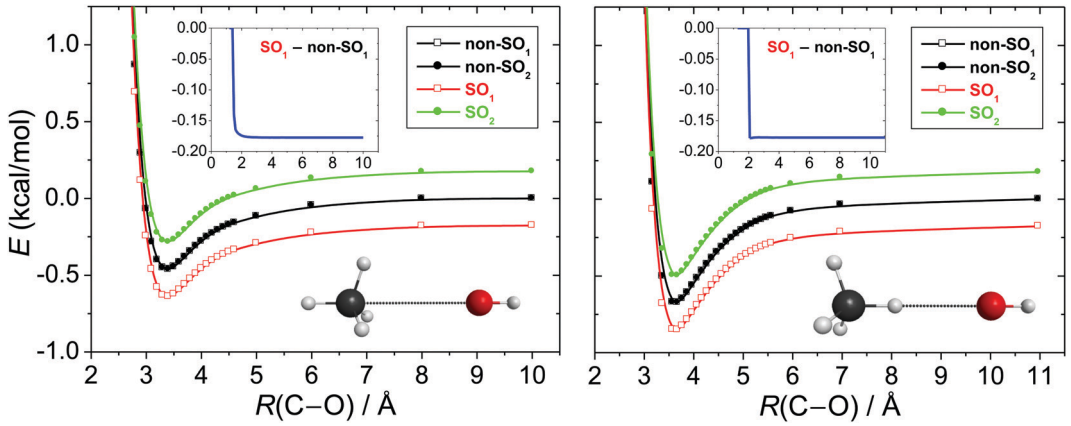

Fig. 5 Potential energy curves along the C_3 axis of the $CH_4\cdots OH$ system obtained at the MRCI+Q/aug-cc-pVDZ level of theory while the structures of the CH_4 and OH units are kept frozen at their equilibrium geometries. SO_1 and SO_2 denote the spin–orbit ground and excited states, whereas non-SO_1 and non-SO_2 are the non-relativistic ground and excited electronic states, respectively. The insets show the distance dependence of the spin–orbit corrections obtained as difference between the SO_1 and non-SO_1 energies.

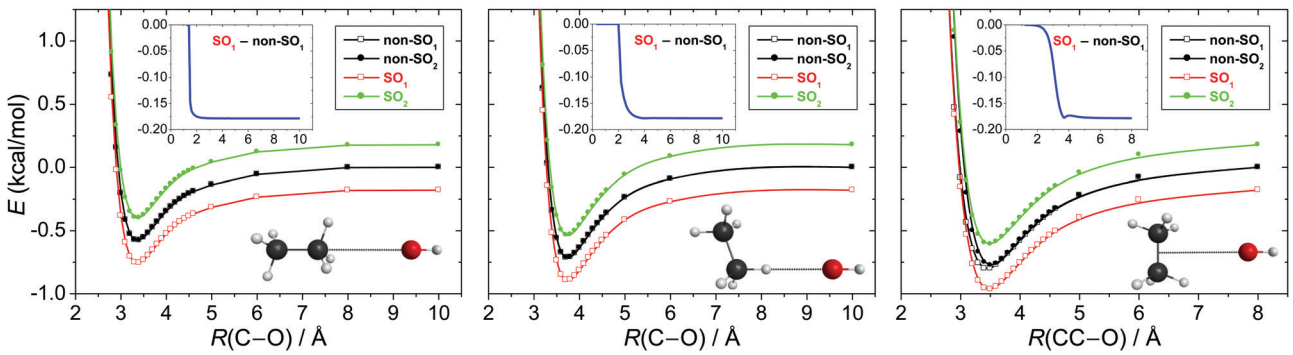

Fig. 6 Potential energy curves along the C_3 (left), CH (middle), and CC-perpendicular (right) axes of the $C_2H_6\cdots OH$ system obtained at the MRCI+Q/aug-cc-pVDZ level of theory while the structures of the C_2H_6 and OH units are kept frozen at their equilibrium geometries. SO_1 and SO_2 denote the spin–orbit ground and excited states, whereas non-SO_1 and non-SO_2 are the non-relativistic ground and excited electronic states, respectively. The insets show the distance dependence of the spin–orbit corrections obtained as difference between the SO_1 and non-SO_1 energies.

significantly larger than the above-mentioned mean deviation between theory and experiment. Furthermore, the excellent agreement for these measurable quantities confirms the accuracy of the present theoretical predictions for the experimentally hardly accessible properties, such as barrier heights.

Table 5 Comparison between the best available experimental and our computed benchmark 0 K reaction enthalpies (kcal mol^{-1}) for the OH + CH_4/C_2H_6 reactions

Reaction	Theory[a]	Experiment[b]
$OH + CH_4 \rightarrow CH_3OH + H$	13.19	13.22 ± 0.04
$OH + CH_4 \rightarrow CH_3 + H_2O$	−14.37	−14.28 ± 0.02
$OH + C_2H_6 \rightarrow C_2H_5OH + H$	7.12	7.13 ± 0.06
$OH + C_2H_6 \rightarrow CH_3OH + CH_3$	−2.20	−2.16 ± 0.05
$OH + C_2H_6 \rightarrow C_2H_5 + H_2O$	−18.19	−18.35 ± 0.07

[a] Benchmark theoretical reaction enthalpies (this work). [b] Data obtained from the latest version (1.122 g) of the Active Thermochemical Tables (ATcT).[61] Uncertainties are derived from the uncertainties of each 0 K enthalpy of formation given in ATcT using the Gaussian error-propagation law.

IV. Summary and conclusions

The reactions of the OH radical with methane and ethane have become benchmark systems to understand the dynamics and mechanisms of polyatomic reactions. Despite many previous experimental and theoretical studies[16–39] focusing on the exothermic (ΔH_0 = −14.37/−18.19 kcal mol^{-1}) hydrogen-abstraction reaction resulting in H_2O + CH_3/C_2H_5 *via* low adiabatic barriers of 4.78/2.18 kcal mol^{-1}, other product channels and their energetic requirements were unknown until the present study. Here, we show that hydrogen-substitution leading to H + CH_3OH/C_2H_5OH is endothermic with ΔH_0 = 13.19/7.12 kcal mol^{-1} and can proceed *via* a Walden-inversion barrier with adiabatic height of 43.53/41.73 kcal mol^{-1} or for the latter we have also found a front-side attack pathways *via* an adiabatic barrier of 52.48 kcal mol^{-1}. For OH + C_2H_6 a methyl-substitution channel forming CH_3 + CH_3OH products is also possible, which is exothermic, ΔH_0 = −2.20 kcal mol^{-1}, but has a large adiabatic barrier of 39.60 kcal mol^{-1}. For the product channel several complexes have been revealed and

characterized, showing a stability order of $HOH\cdots C_2H_5$, $HOH\cdots CH_3$, $H_3C\cdots CH_3OH$, and $H\cdots C_2H_5OH$ with D_e values of 2.4, 1.7, 0.7, and 0.3 kcal mol^{-1}, respectively. For the first time, we have performed SO computations for the entrance channel, thereby revealing van der Waals wells with depths of 0.5–0.8 kcal mol^{-1} depending on the relative orientation of the reactants. Unlike for the halogen + CH_4/C_2H_6 systems,[13,14] the well is the deepest for perpendicular C–C$\cdots$OH approach (0.8 kcal mol^{-1}), followed by the $H_3CH/H_3CH_2CH\cdots OH$ (0.7 kcal mol^{-1}) and $HCH_3/H_3CCH_3\cdots OH$ (0.5–0.6 kcal mol^{-1}) arrangements. These pre- and post-reaction wells may play significant roles in the dynamics of the hydrogen-abstraction processes, especially at low collision energies, by steering the reactants in the entrance channels and affecting product rotation in the exit channels, respectively.

The stationary-point properties have been computed using an accurate composite *ab initio* approach which goes beyond the widely-used standard quantum chemistry. The complete-basis-set limit of CCSD(T) is approached well within 0.1 kcal mol^{-1} with explicitly-correlated CCSD(T)-F12b/aug-cc-pV*n*Z computations with $n = 5$ and 4(Q) for OH + CH_4 and OH + C_2H_6, respectively. Post-CCSD(T) correlation (-0.9 to -0.1), core correlation (-0.1 to +0.4), scalar relativistic (+0.0 to +0.2), SO (+0.2), and ZPE (-2 to -1) effects are determined resulting in typical values for the title reactions as indicated in parentheses in kcal mol^{-1}. We conclude that the present theoretical predictions provide sub-chemically accurate relative energies with an estimated uncertainty of around 0.1 kcal mol^{-1}, which is about an order of magnitude better than that of the standard quantum chemistry studies. The outstanding accuracy of the present results can be confirmed by the comparison of the computed reaction enthalpies with the corresponding experimental data[61] showing only 0.07 kcal mol^{-1} mean absolute deviation.

The new insights into the mechanisms and alternative reaction pathways of the title reactions are essential to develop global PESs for the OH + CH_4/C_2H_6 systems, allowing dynamical investigations over a large collision energy range. Furthermore, the relative energies of the stationary points may guide future experimental investigations showing the thermodynamical and kinetical controls of the different processes. Finally, the present composite approach may be utilized in several similar *ab initio* investigations if high accuracy is desired.

Conflicts of interest

There are no conflicts of interest to declare.

Acknowledgements

We thank the National Research, Development and Innovation Office-NKFIH, K-125317, the Ministry of Human Capacities, Hungary grant 20391-3/2018/FEKUSTRAT, and the Momentum (Lendület) Program of the Hungarian Academy of Sciences for financial support.

References

1 C. Murray and A. J. Orr-Ewing, *Int. Rev. Phys. Chem.*, 2004, **23**, 435.
2 E. S. Whitney, A. M. Zolot, A. B. McCoy, J. S. Francisco and D. J. Nesbitt, *J. Chem. Phys.*, 2005, **122**, 124310.
3 W. Li, C. S. Huang, M. Patel, D. Wilson and A. Suits, *J. Chem. Phys.*, 2006, **124**, 011102.
4 D. Troya, G. C. Schatz, D. J. Garton, A. L. Brunsvold and T. K. Minton, *J. Chem. Phys.*, 2004, **120**, 731.
5 R. J. Holiday, C. H. Kwon, C. J. Annesley and F. F. Crim, *J. Chem. Phys.*, 2006, **125**, 133101.
6 H. A. Bechtel, Z. H. Kim, J. P. Camden and R. N. Zare, *J. Chem. Phys.*, 2004, **120**, 791.
7 K. Liu, *J. Chem. Phys.*, 2015, **142**, 080901.
8 B. Fu, X. Shan, D. H. Zhang and D. C. Clary, *Chem. Soc. Rev.*, 2017, **46**, 7625.
9 J. Espinosa-Garcia, J. C. Corchado, M. Garcia-Chamorro and C. Rangel, *Phys. Chem. Chem. Phys.*, 2018, **20**, 19860.
10 F. Meng, W. Yan and D. Wang, *Phys. Chem. Chem. Phys.*, 2012, **14**, 13656.
11 Z. Chen, J. Chen, R. Chen, T. Xie, X. Wang, S. Liu, G. Wu, D. Dai, X. Yang and D. H. Zhang, *Proc. Natl. Acad. Sci. U. S. A.*, 2020, **117**, 9202.
12 R. Welsch and U. Manthe, *J. Chem. Phys.*, 2015, **142**, 064309.
13 G. Czakó and J. M. Bowman, *J. Phys. Chem. A*, 2014, **118**, 2839.
14 D. Papp, B. Gruber and G. Czakó, *Phys. Chem. Chem. Phys.*, 2019, **21**, 396.
15 G. Czakó, T. Győri, B. Olasz, D. Papp, I. Szabó, V. Tajti and D. A. Tasi, *Phys. Chem. Chem. Phys.*, 2020, **22**, 4298.
16 B. Jiang and H. Guo, *J. Chin. Chem. Soc.*, 2014, **61**, 847.
17 D. L. Baulch, R. J. B. Craven, M. Din, D. D. Drysdale, S. Grant, D. J. Richardson, A. Walker and G. Watling, *J. Chem. Soc., Faraday Trans. 1*, 1983, **79**, 689.
18 F. P. Tully, A. T. Droege, M. L. Koszykowski and C. F. Melius, *J. Phys. Chem.*, 1986, **90**, 691.
19 K. D. Dobbs, D. A. Dixon and A. Komornicki, *J. Chem. Phys.*, 1993, **98**, 8852.
20 L. N. Krasnoperov and J. V. Michael, *J. Phys. Chem. A*, 2004, **108**, 5643.
21 N. I. Butkovskaya and D. W. Setser, *Int. Rev. Phys. Chem.*, 2003, **22**, 1.
22 J. Espinosa-Garcia and J. C. Corchado, *Theor. Chem. Acc.*, 2015, **134**, 6.
23 F. Khaled, B. R. Giri, M. Szőri, B. Viskolcz and A. Farooq, *Chem. Phys. Lett.*, 2015, **641**, 158.
24 M. Tsiouris, M. D. Wheeler and M. I. Lester, *Chem. Phys. Lett.*, 1999, **302**, 192.
25 L. Bonnet and J. Espinosa-Garcia, *Chem. Phys. Lett.*, 2018, **711**, 184.
26 S. Rudić, J. M. Merritt and R. E. Miller, *Phys. Chem. Chem. Phys.*, 2009, **11**, 5345.
27 T. Hashimoto and S. Iwata, *J. Phys. Chem. A*, 2002, **106**, 2652.
28 J. P. Senosiain, C. B. Musgrave and D. M. Golden, *J. Phys. Chem. A*, 2001, **105**, 1669.
29 B. Zhang, W. Shiu and K. Liu, *J. Phys. Chem. A*, 2005, **109**, 8983.

30 J. Korchowiec, S. Kawahara, K. Matsumura, T. Uchimaru and M. Sugie, *J. Phys. Chem. A*, 1999, **103**, 3548.
31 H. Lin, Y. Zhao, B. A. Ellingson, J. Pu and D. G. Truhlar, *J. Am. Chem. Soc.*, 2005, **127**, 2830.
32 P. L. Raston, E. I. Obi and G. E. Douberly, *J. Phys. Chem. A*, 2017, **121**, 7597.
33 B. A. Ellingson, J. Pu, H. Lin, Y. Zhao and D. G. Truhlar, *J. Phys. Chem. A*, 2007, **111**, 11706.
34 Y. Benitez, D. Lu, K. G. Lunny, J. Li, H. Guo and R. E. Continetti, *J. Phys. Chem. A*, 2019, **123**, 4825.
35 L. Masgrau, Á. González-Lafont and J. M. Lluch, *J. Chem. Phys.*, 2001, **115**, 4515.
36 M. Tsiouris, M. D. Wheeler and M. I. Lester, *J. Chem. Phys.*, 2001, **114**, 187.
37 M. D. Wheeler, M. Tsiouris, M. I. Lester and G. Lendvay, *J. Chem. Phys.*, 2000, **112**, 6590.
38 J. Li and H. Guo, *J. Chem. Phys.*, 2015, **143**, 221103.
39 H. Song, Y. Lu, J. Li, M. Yang and H. Guo, *J. Chem. Phys.*, 2016, **144**, 164303.
40 T. B. Adler, G. Knizia and H.-J. Werner, *J. Chem. Phys.*, 2007, **127**, 221106.
41 C. Møller and M. S. Plesset, *Phys. Rev.*, 1934, **46**, 618.
42 T. H. Dunning, Jr., *J. Chem. Phys.*, 1989, **90**, 1007.
43 K. Raghavachari, G. W. Trucks, J. A. Pople and M. Head-Gordon, *Chem. Phys. Lett.*, 1989, **157**, 479.
44 J. Noga and R. J. Bartlett, *J. Chem. Phys.*, 1987, **86**, 7041.
45 M. Kállay and J. Gauss, *J. Chem. Phys.*, 2005, **123**, 214105.
46 J. G. Hill, S. Mazumder and K. A. Peterson, *J. Chem. Phys.*, 2010, **132**, 054108.
47 M. Douglas and N. M. Kroll, *Ann. Phys.*, 1974, **82**, 89.
48 A. Berning, M. Schweizer, H.-J. Werner, P. J. Knowles and P. Palmieri, *Mol. Phys.*, 2000, **98**, 1823.
49 S. R. Langhoff and E. R. Davidson, *Int. J. Quantum Chem.*, 1974, **8**, 61.
50 K. R. Shamasundar, G. Knizia and H.-J. Werner, *J. Chem. Phys.*, 2011, **135**, 054101.
51 R. D. Amos, J. S. Andrews, N. C. Handy and P. J. Knowles, *Chem. Phys. Lett.*, 1991, **185**, 256.
52 G. Knizia, T. B. Adler and H.-J. Werner, *J. Chem. Phys.*, 2009, **130**, 054104.
53 H.-J. Werner, P. J. Knowles, G. Knizia, F. R. Manby and M. Schütz, *et al.*, Molpro, version 2015.1, a package of *ab initio* programs, see http://www.molpro.net.
54 Mrcc, a quantum chemical program suite written by M. Kállay, Z. Rolik, I. Ladjánszki, L. Szegedy, B. Ladóczki, J. Csontos and B. Kornis, see also Z. Rolik and M. Kállay, *J. Chem. Phys.*, 2011, **135**, 104111, as well as: www.mrcc.hu.
55 G. S. Hammond, *J. Am. Chem. Soc.*, 1955, **77**, 334.
56 A. Chattopadhyay, S. Tasaki, R. Bersohn and M. Kawasaki, *J. Chem. Phys.*, 1991, **95**, 1033.
57 Z. Zhao, Z. Zhang, S. Liu and D. H. Zhang, *Nat. Commun.*, 2017, **8**, 14506.
58 G. Czakó and J. M. Bowman, *J. Chem. Phys.*, 2012, **136**, 044307.
59 G. Czakó, *J. Phys. Chem. A*, 2012, **116**, 7467.
60 L. Krotos and G. Czakó, *J. Phys. Chem. A*, 2017, **121**, 9415.
61 B. Ruscic and D. H. Bross, *Active Thermochemical Tables (ATcT) values based on ver. 1.122g of the Thermochemical Network*, Argonne National Laboratory, 2019, available at ATcT.anl.gov.